RSC Advances

PAPER

View Article Online
View Journal | View Issue

Check for updates

Cite this: *RSC Adv.*, 2021, **11**, 29543

Viologen–cucurbituril host/guest chemistry – redox control of dimerization *versus* inclusion†

Parastoo Dalvand,[a] Katia Nchimi Nono,[b] Dinesh Shetty,[c] Farah Benyettou,[d] Zouhair Asfari,[e] Carlos Platas-Iglesias,[f] Mark A. Olson,[g] Ali Trabolsi *[d] and Mourad Elhabiri *[a]

Received 17th July 2021
Accepted 9th August 2021

DOI: 10.1039/d1ra05488k

rsc.li/rsc-advances

Two calix[4]arene systems, **C23**$^{4+}$ and **C24**$^{4+}$ – where 2 corresponds to the number of viologen units and 3–4 corresponds to the number of carbon atoms connecting the viologen units to the macrocyclic core – have been synthesized and led to the formation of [3]pseudorotaxanes when combined with either **CB[7]** or **CB[8]**. The [3]pseudorotaxanes spontaneously dissociate upon reduction of the bipyridinium units as the result of intramolecular dimerization of the two face-to-face viologen radical cations. **CB[7]** and **CB[8]**-based [2]pseudorotaxanes containing monomeric viologen guest model compounds, **MC3**$^{2+}$ and **MC**$^{4+}$, do not undergo decomplexation and dimerization following electrochemical reduction of their bipyridinium units.

Introduction

The stimuli–responsive properties of a molecule with redox-active units can be advantageously used in a broad range of applications including drug delivery and development, electronic displays, electronic memory, batteries, and multi-state switchable materials.[1–11] Among these redox-active molecules, for example metallocenes, tetrathiafulvalene derivatives, naphthalene diimides, and benzoquinones, bipyridinium derivatives[12] (also known as viologens) are of particular interest because of their vibrant electrochromic properties. Bipyridinium dications (**BIPY**$^{2+}$), for example, are typically colorless whereas **BIPY**$^{\bullet+}$ radical monocations[13] are deep blue in color.[14] Furthermore, these radical cations spontaneously undergo π-dimerization, a process known as pimerization[15] that is driven by radical–radical interactions that favor the formation of the singlet state (*i.e.*, panchromatic absorption)[14–16] to afford the (**BIPY**$^{\bullet+}$)$_2$ dimer in aqueous solution. Pimerization of **BIPY**$^{\bullet+}$ radical cations has been used in supramolecular and mechanostereochemical systems to generate translational and rotational molecular movement in many recently reported mechanically interlocked molecules.[17–19] Furthermore, the rich redox chemistry of viologens also makes them attractive for use in electrochromic, catalytic, and bioanalytical applications.[20–22]

However, one major complication that limits the use of viologen-based pimerization to develop stimuli–responsive materials is that the system suffers from low dimerization constants (*e.g.*, log $K_{Dim} = 2.70$).[23] This results in loosely associated π-dimers in solution, and thus requires the use of high concentrations of the constituent molecular components to drive the binding. The use of low temperatures, micelle environments,[24] or macrocyclic hosts with large cavity sizes such as cucurbiturils (*e.g.*, **CB[8]**), cyclodextrins (*e.g.*, β-CD), or Stoddart's Blue Box[17,18,25] can help favor the formation of intermolecular π-dimer species. A. E. Kaifer, K. Kim and their coworkers described for the first time the interaction of **MV**$^{2+}$ with cucurbit[*n*]uril hosts such as **CB[7]** and **CB[8]**.[26–28] With **CB[8]**, it was found that **MV**$^{2+}$ strongly binds in a 1 : 1 stoichiometry inside the macrocycle cavity, the major driving force being ion–dipole interactions between the positively charged viologen and the oxygen rich host portals atoms. One electron reduction of methyl viologen **MV**$^{2+}$ allowed the formation of a bisradical species ((**MV**$^{\bullet+}$)$_2$⊂**CB[8]**). The dimerization constant of the **MV**$^{\bullet+}$ in the presence of the **CB[8]** was estimated to be ~2×10^7 M^{-1} which is about 10^5 times larger than **MV**$^{\bullet+}$ alone.[28,29]

[a]*Université de Strasbourg, Université de Haute-Alsace, CNRS, LIMA, UMR 7042, Equipe Chimie Bioorganique et Médicinale, ECPM, 25 Rue Becquerel, 67000 Strasbourg, France. E-mail: elhabiri@unistra.fr*

[b]*Department of Inorganic Chemistry, Faculty of Science, University of Yaoundé 1, Yaoundé, Cameroon*

[c]*Department of Chemistry & Center for Catalysis and Separation (CeCaS), Khalifa University, Abu Dhabi, United Arab Emirates*

[d]*New York University Abu Dhabi (NYUAD), Experimental Research Building, Building C1, Saadiyat Island, Abu Dhabi, United Arab Emirates. E-mail: ali.trabolsi@nyu.edu*

[e]*Equipe de Synthèse Pour l'Analyse (SynPA), Institut Pluridisciplinaire Hubert Curien (IPHC), UMR 7178 CNRS/Université de Strasbourg, ECPM, Bâtiment R1N0, 25-rue Becquerel, 67087 Strasbourg Cedex 2, France*

[f]*Universidade da Coruña, Centro de Investigacións Científicas Avanzadas (CICA), Departamento de Química, Facultade de Ciencias, 15071 A Coruña, Galicia, Spain*

[g]*Northwestern University, Department of Chemistry, 2145 Sheridan Rd, Evanston, Illinois, USA*

† Electronic supplementary information (ESI) available: Physicochemical characterisation, spectrophotometric titrations, Job's plots, NMR, MS and EPR spectra, and DFT structures. See DOI: 10.1039/d1ra05488k

Open Access Article. Published on 02 September 2021. Downloaded on 4/18/2026 12:09:39 PM. This article is licensed under a Creative Commons Attribution-NonCommercial 3.0 Unported Licence.

Open Access Article. Published on 02 September 2021. Downloaded on 4/18/2026 12:09:39 PM. This article is licensed under a Creative Commons Attribution-NonCommercial 3.0 Unported Licence.

Supramolecular assemblies based on **CB[8]** have been reviewed recently by A. E. Kaifer, M. D. Garcia *et al.*[30]

Alternatively, it has been shown that pre-organizing two or more organic radicals with well-tailored anchoring platforms and appropriate chain lengths can strengthen the intramolecular binding of the π-dimers in solution.[31] We have previously demonstrated that a hexavalent phosphazene[30] fulfilled most of the prerequisites including ease of functionalization, and exhibited efficient and fast pimerization. This compound was applicable towards electrochromic material research and possessed specific recognition properties as a function of the viologen redox state. In addition, alkyl,[32–37] porphyrinic,[38,39] ferrocenyl,[40] aryl,[32–44] C_{60},[45] and calixarene[46,47] linkers, as well as dendritic[48,49] and covalent organic polymeric[50,51] viologen-based materials (Scheme S1 in the ESI†) have also been demonstrated to promote intramolecular dimerization of their corresponding bipyridinium radical cations.

In line with our ongoing research on viologen-based systems for generating redox-active devices, we turned our attention to calix[4]arene as an inert anchoring platform. Calix[4]arenes can be easily chemically modified and their structural and conformational properties make for an excellent foundation upon which to build increasingly complex architectures. Calix[4]arene can exist in four conformations in solution, the cone, the partial cone, the 1,2-alternate, and the 1,3-alternate. Furthermore, the alkylation selectivity, in regard to the number of substituted phenols, can be controlled by the reaction conditions, thereby giving rise to a broad range of conformers and cavity sizes.[52]

Herein, we report the synthesis and physicochemical characterization of a series of host–guest monomeric and calix[4]arene-functionalized dimeric viologen⊂**CB**-based pseudorotaxane complexes and the structure–property relationships that enable their electrochemical-triggered decomplexation. Calix[4]arene was functionalized with two terminal viologens using spacers of varying length (Fig. 1).[45] The use of synthetic receptors that have both a high affinity and a high selectivity for the binding of guests in water is indeed a very interesting prospect.[53–56] The recognition properties of the viologen-based systems (oxidized and reduced) with **CB[7]** and **CB[8]** were analyzed using a set of complementary analytical methods which include ESI-MS, square wave and cyclic voltammetry, UV-visible-near infrared (NIR) spectrophotometry, ^{1}H-NMR, and electron paramagnetic resonance (EPR).

Experimental section

Synthesis

Starting materials and solvents. All commercial reagents were purchased from Sigma-Aldrich and used without further purification. 1-Methyl-[4,4′-bipyridin]-1-ium iodide (**I1**) was prepared according to literature procedures.[57] 1-(3-Bromopropoxy)-4-(*tert*-butyl)benzene (**I2**), 1-(4-bromo-butoxy)-4-(*tert*-butyl)benzene (**I3**), 1,3-bis(3-bromopropoxy)-*p*-*tert*-butyl-calix[4]arene (**I5**) and 1,3-bis(4-bromobutoxy)-*p*-*tert*-butyl-calix[4]arene (**I6**) were also prepared according reported procedures with slight modifications.[58,59] The dicationic dimethyl viologen **MV·2I** (Fig. 1)[12] and tetrakis-*p*-*tert*-butyl-calix[4]arene **I4** (ref. 60 and 61) were prepared according to literature procedures. Thin layer chromatography (TLC) was used to follow the reactions and was performed on aluminium sheets bearing silica gel 60 F254 (E. Merck). Column chromatography was performed using silica gel (Merck; 40–63 μm). Nuclear magnetic resonance (NMR) spectra were recorded on a Bruker AC 400 with working frequencies of 400 and 100 MHz for ^{1}H and ^{13}C, respectively. Chemical shifts are reported in ppm relative to the signals corresponding to the residual non-deuterated solvents ($CDCl_3$ (δ = 7.26), CD_3OD (δ = 3.34), and d_6-DMSO (δ = 2.50). High-resolution electrospray mass (HR-ESI) spectra were measured on a micro Q-TOF (Bruker) spectrometer.

1-(3-4-(*Tert*-butyl)phenoxy)propyl)-1-methyl-[4,4′-bipyridin]-1,1′-diium bromide iodide (MC3^{2+}). 0.8 g (2.95 mmol) of **I2** was mixed with 0.88 g (2.95 mmol) of **I1** in 30 mL of acetonitrile (CH_3CN) and the mixture was refluxed for two days. The reaction mixture was filtered and washed with CH_3CN to afford **MC3**$^{2+}$ as a red-orange solid (yield: 31%). ^{1}H NMR (400 MHz, CD_3OD): δ [ppm]: 9.36 [d, 2H, J = 6.8 Hz, Ar-H], 9.23 [d, 2H, J = 6.8 Hz, Ar-H], 8.70 [t, 4H, J = 7.2 Hz, Ar-H], 7.30 [d, 2H, J = 8.8

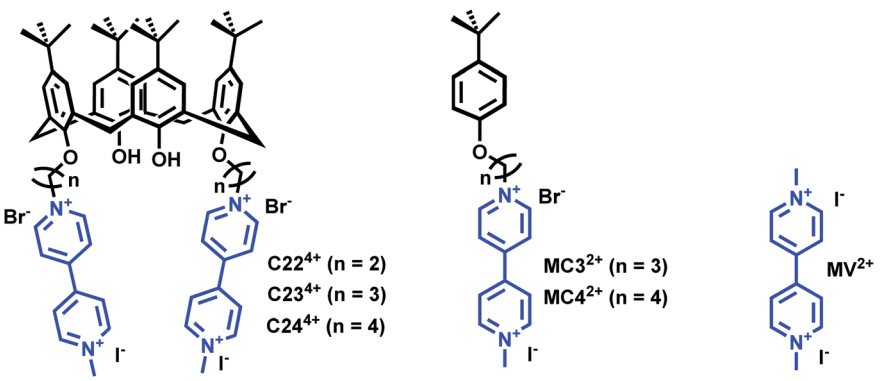

Fig. 1 Chemical structures of the calix[4]arene viologen-based systems C23^{4+} and C24^{4+} and the reference compounds MC3^{2+} and MC4^{4+}. The number 2 stands for the number of viologens while 3–4 correspond to the number of carbons of the chain connecting the terminal viologens to the calix[4]arene backbone. Methyl-viologen (MV^{2+}) has been used as a model compound in this work. C22^{4+} (PF_6^- salt) was not synthesized in this work (see ref. 45) and only considered for DFT calculations.

© 2021 The Author(s). Published by the Royal Society of Chemistry

Open Access Article. Published on 02 September 2021. Downloaded on 4/18/2026 12:09:39 PM. This article is licensed under a Creative Commons Attribution-NonCommercial 3.0 Unported Licence.

Ar-H], 6.77 [d, 2H, $J = 9.2$, Ar-H], 5.04 [t, 2H, $J = 6.8$ Hz, N–CH_2–CH_2], 4.57 [s, 3H, N–CH_3], 4.19 [t, 2H, $J = 5.6$ Hz, O–CH_2–CH_2], 2.66–2.60 [m, 2H, N–CH_2–CH_2–CH_2–O], 1.29 [s, 9H, $C(CH_3)_3$]. ^{13}C NMR (100 MHz, CD_3OD): δ [ppm]: 158.08, 152.66, 152.21, 151.75, 148.88, 148.34, 145.96, 129.04, 128.84, 128.20, 124.39, 115.78, 66.58, 62.13, 35.75, 32.78. Melting point: 258–9 °C. HR-MS for $C_{24}H_{30}ON_2$ [**MC3**$^{2+}$]: calcd $m/z = 181.1174$ and exp. $m/z = 181.1172$.

1-(4-4-(*Tert*-butyl) phenoxy)butyl)-1′-methyl-[4,4′-bipyridin]-1,1′-diium bromide iodide (MC4^{2+}). 1.58 g (5.53 mmol) of **I3** was mixed with 1.5 g (5.02 mmol) of **I1** in 30 mL of CH_3CN and the mixture was refluxed for three days. The reaction mixture was filtered and washed with CH_3CN to afford **MC4**$^{2+}$ as a yellow-orange solid (yield: 71%). ^{1}H NMR (400 MHz, CD_3OD): δ [ppm]: 9.36 [d, 2H, $J = 7.2$ Hz, Ar-H], 9.23 [d, 2H, $J = 6.8$ Hz, Ar-H], 8.73 [d, 2H, $J = 6.8$ Hz, Ar-H], 8.70 [d, 2H, $J = 6.8$ Hz, Ar-H], 7.32 [d, 2H, $J = 8.8$ Ar-H], 6.88 [d, 2H, $J = 8.8$, Ar-H], 4.90 [t, 2H, $J = 7.6$ Hz, N–CH_2–CH_2], 4.57 [s, 3H, N–CH_3], 4.10 [t, 2H, $J = 6$, CH_2–O–Ar], 2.39–2.32 [m, 2H, N–CH_2–CH_2–CH_2], 2.00–1.93 [m, 2H, O–CH_2–CH_2–CH_2], 1.31 [s, 9H, $C(CH_3)_3$]. ^{13}C NMR (100 MHz, CD_3OD): δ [ppm]: 158.73, 152.13, 148.64, 148.01, 145.52, 129.21, 128.84, 128.09, 115.94, 69.03, 63.95, 35.70, 32.80, 30.55, 27.92. Melting point: 254–5 °C. HR-MS for $C_{25}H_{32}ON_2$ [**MC4**$^{2+}$]: calcd $m/z = 188.1252$ and exp. $m/z = 188.1245$.

1,3-Bis(3-(1′-methyl-[4,4′-bipyridin]-1,1′-diium)propoxy)-*p*-*tert*-butyl-calix[4]-arene dibromide diiodide (C23^{4+}). 1.192 g (4 mmol) of **I1** was added to the flask containing 0.365 g (0.4 mmol) of **I5** and 30 mL of CH_3CN. The mixture was left under reflux for 3 days. The solvent was fully removed under vacuum. The product (**C23**$^{4+}$, red-orange solid, yield: 85%) was washed with water, filtrated, and dried under vacuum. ^{1}H NMR (400 MHz, CD_3OD): δ [ppm]: 9.60 [d, 4H, $J = 6.8$ Hz, Ar-H], 9.22 [d, 4H, $J = 6.8$ Hz, Ar-H], 8.82 [d, 4H, $J = 5.6$ Hz, Ar-H], 8.74 [d, 4H, $J = 6.8$ Hz, Ar-H], 7.22 [s, 4H, Ar(calix)-H], 7.07 [s, 4H, Ar(calix)-H], 5.30 [t, 4H, $J = 7.2$ Hz, N–CH_2–CH_2], 4.56 [s, 6H, N–CH_3], 4.32–4.23 [d, 8H, Ar-CH_2-Ar and CH_2–O-Ar], 3.50 [d, 4H, $J = 13.6$, Ar-CH_2-Ar], 3.02–2.95 [m, 4H, CH_2–CH_2–CH_2], 1.30 [s, 18H, $C(CH_3)_3$], 1.02 [s, 18H, $C(CH_3)_3$]. ^{13}C NMR (100 MHz, d_6-DMSO): δ [ppm]: 150.65, 150.36, 149.54, 148.80, 148.26, 147.52, 146.77, 142.61, 133.91, 128.37, 127.70, 127.00, 126.662, 126.31, 73.26, 58.88, 49.04, 34.92, 37.55, 32.39, 32.29, 31.76, 31.61. Melting point: 295–6 °C. HR-MS for $C_{72}H_{88}O_4N_4$ [**C23**$^{4+}$ + 2e$^-$]:$^{2+}$ calcd $m/z = 536.3397$ and exp. $m/z = 536.3382$.

1,3-Bis(3-(1′-methyl-[4,4′-bipyridin]-1,1′-diium)butoxy)-*p*-*tert*-butyl-calix[4]arene dibromide diiodide (C24^{4+}). 0.368 g (0.4 mmol) of **I6** was dissolved in 30 mL of CH_3CN. 1.192 g (4 mmol) of **I1** was added. The mixture was left under reflux for 3 days. The solvent was fully removed under vacuum. The product obtained as an orange solid (**C24**$^{4+}$, yield: 67%) was washed with water (due to its poor solubility in water), filtrated and dried under vacuum. ^{1}H NMR (400 MHz, CD_3OD): δ [ppm]: 9.54 [d, 4H, $J = 6.4$ Hz, Ar-H], 9.21 [d, 4H, $J = 6.4$ Hz, Ar-H], 8.78 [d, 4H, $J = 6.4$ Hz, Ar-H], 8.71 [d, 4H, $J = 6.8$ Hz, Ar-H], 7.19 [s, 4H, Ar(calix)-H], 7.05 [s, 4H, Ar(calix)-H], 5.15 [t, 4H, $J = 7.6$ Hz, N–CH_2–CH_2], 4.56 [s, 6H, N–CH_3], 4.32 [d, 4H, $J = 12.8$, Ar-CH_2-Ar], 4.16 [t, 4H, $J = 6.8$ Hz, CH_2–O-Ar], 3.48 [d, 4H, $J = 12.8$, Ar-CH_2-Ar], 2.66–2.58 [m, 4H, N–CH_2–CH_2–], 2.25–2.17[m, 4H, –CH_2–CH_2–O], 1.29 [s, 18H, $C(CH_3)_3$], 1.02 [s, 18H, $C(CH_3)_3$]. ^{13}C NMR (100 MHz, DMSO): δ [ppm]: 150.79, 150.46, 149.51, 148.89, 148.10, 147.48, 146.74, 142.42, 134.02, 128.41, 127.57, 127.01, 126.56, 126.21, 76.01, 61.22, 49.02, 34.92, 34.52, 32.29, 31.79. Melting point: 224–5 °C. HR-MS for $C_{74}H_{92}O_4N_4$ [**C24**$^{4+}$ + 2e$^-$]$^{2+}$: calcd $m/z = 550.3554$ and exp. $m/z = 550.3561$.

Physico-chemistry. The experimental details and related figures are given in the ESI.†

DFT calculations. The singlet states of the **C22**$^{2(\cdot+)}$, **C23**$^{2(\cdot+)}$ and **C24**$^{2(\cdot+)}$ systems were investigated using DFT calculations within the hybrid *meta*-GGA approximation with the M06-2X functional[62] and the Gaussian 16 package.[63] The standard 6-311G(d,p) basis set was used throughout. Solvent effects (water) were incorporated with the polarized continuum model (PCM) using default settings and the integral equation formalism.[64] Frequency calculations were used to confirm that the optimized geometries corresponded to local energy minima on the potential energy surface. The M06-2X/6-311G(d,p) approach in combination with the PCM was found to provide good results for the description of π-stacking interactions of viologen derivatives.[65]

EPR spectroscopy. EPR spectra were recorded on a CMS 800 EPR spectrometer 8400 and measurements were carried out with solutions of the calixarene-bis-viologens compounds **C23**$^{4+}$ and **C24**$^{4+}$, along with their model ligands, namely **MC3**$^{2+}$ and **MC4**$^{2+}$, in the absence and in the presence of **CB[7]**. This study was performed to evaluate whether or not the radical cations were dimerized or segregated[66] depending on the composition of the mixture. The radical cations species were produced chemically by addition of an excess of a reducing agent (*e.g.*, sodium dithionite $Na_2S_2O_4$). Each solution was prepared at a concentration of $\sim 10^{-4}$ M. The EPR data are available in Fig. S17–S20 in the ESI.†

Electrochemistry. All the solutions used for the electrochemical experiments were prepared from 0.1 M TBACl aqueous solution with following concentrations of each species: **MC4**$^{2+}$ ($C = 6.3 \times 10^{-5}$ M), **MC3**$^{2+}$ ($C = 6 \times 10^{-5}$ M), **C24**$^{4+}$ ($C = 5 \times 10^{-5}$ M), and **C23**$^{4+}$ ($C = 5 \times 10^{-5}$ M) with **CB[7]** ($C = 2 \times 10^{-4}$ M). The setup comprises a Gamry Multipurpose instrument (Reference 600) interfaced to a PC. The experiments were performed using a glassy carbon working electrode (0.071 cm^2, BASi). The electrode surface was polished routinely with 0.05 μm alumina–water slurry on a felt surface immediately before use. The counter electrode was a Pt coil and the reference electrode was a Ag/AgCl electrode. Cyclic voltammetry (CV) and square wave (SW) differential pulse voltammetry were carried out at room temperature in an argon-purged H_2O solution between 0 V (initial potential) and −1.2 V (final potential). Chronocoulometry experiments were performed upon stepping from 0 to −0.7 V for 10 s before measuring the response signal corresponding to a radical-cation. Then the potential is stepped from −0.7 V to 0 V allowing measurement of the response signal corresponding to the fully oxidized species. The experimental errors on the potential values are ±10 mV.

Open Access Article. Published on 02 September 2021. Downloaded on 4/18/2026 12:09:39 PM. This article is licensed under a Creative Commons Attribution-NonCommercial 3.0 Unported Licence.

Results and discussion

Synthesis

Two calix[4]arene systems, namely **C23**$^{4+}$ and **C24**$^{4+}$, whereby 2 stands for the number of viologens and 3–4 correspond to the number of carbons of the chain connecting the viologens to the calix[4]arene core (Scheme 1), were synthesized. For a deeper understanding of the host–guest complexation properties of the viologen derivatives with either **CB[7]** or **CB[8]**, two model compounds, namely **MC3**$^{2+}$ and **MC4**$^{2+}$, were also prepared. 4,4′-bipyridine was first monomethylated using 1 equivalent of methyl iodide in acetone leading to **I1** with 63% yield. *Tert*-butyl-phenol was reacted either with 1,3-dibromo-propane or 1,4-dibromo-butane in acetone in the presence of 1 equivalent of potassium carbonate to provide intermediates **I2** or **I3**, respectively. The synthesis of **MC3**$^{2+}$ and **MC4**$^{2+}$ was then achieved following the reaction of **I2** or **I3** with 1-methyl-4,4′-bipyridinium (**I1**) in CH_3CN. The synthesis of the tetrakis-*p*-*tert*-butyl-calix[4]arene **I4** (63% yield) was achieved by reaction of *p*-*tert*-butyl-phenol with excess of formaldehyde in the presence of NaOH. As described above, **I4** was then reacted with 1,3-dibromo-propane and 1,4-dibromo-butane to lead to intermediates **I5** (92% yield) or **I6** (65% yield), respectively. Reacting these two calix[4]arene intermediates with **I1** then leads to the targeted bis-viologen systems **C23**$^{4+}$ (85% yield) and **C24**$^{4+}$ (67% yield). All these viologen derivatives were isolated in the form of mixed iodide/bromide salts.

Characterization of the thread/CB[7] [*n*]pseudorotaxanes

Recognition of MC3^{2+} **and MC4**$^{2+}$ **by CB[7].** The UV-vis absorption spectrophotometric binding titration of **MC3**$^{2+}$ (Fig. S1 and S2 in the ESI†) and **MC4**$^{2+}$ (Fig. S3 and S4 in the ESI†) with **CB[7]** and their corresponding Job plots provided evidence that **MC3**$^{2+}\subset$**CB[7]** and **MC4**$^{2+}\subset$**CB[7]** exist as 1 : 1 stoichiometric host–guest complexes. Both **MC3**$^{2+}$ and **MC4**$^{2+}$ are characterized by two main absorptions at ∼225 nm and 260 nm (Table 1) that are attributed to the π–π* transitions of the *tert*-butyl-phenyl and **BIPY**$^{2+}$ chromophoric units, respectively. It was observed that complexation with **CB[7]** induces a hypochromic shift of the absorption band attributed to the **BIPY**$^{2+}$ transitions, while those of the *tert*-butyl-phenyl units remain almost unaltered. This suggested that **CB[7]** is bound to the **BIPY**$^{2+}$ subunit rather than the apparently more hydrophobic alkoxy-*tert*-butyl-phenyl group. This binding behavior is most likely explained by the weaker affinity[67] of the alkoxy-*tert*-butyl-phenyl moiety for **CB[7]** and steric hindrance of its bulky *tert*-butyl group. The calculated binding constants ($\log K_{\mathbf{MC3}^{2+}\subset\mathbf{CB[7]}} = 4.51(6)$ and $\log K_{\mathbf{MC4}^{2+}\subset\mathbf{CB[7]}} = 4.68(5)$ determined in 0.1 M phosphate buffer, pH 7.0) were found to be lower than that determined for **MV**$^{2+}$, most likely as a consequence of statistical effects. In this case, the two pyridinium aromatic faces of **MV**$^{2+}$ are not sterically blocked to **CB[7]**, while one side of the bipyridinium units of **MC**$^{3+}$ and **MC**$^{4+}$ are capped with a *tert*-butyl-phenyl bulky stopper. Consequently, the $K_{\mathbf{MC3}^{2+}}/K_{\mathbf{MV}^{2+}}$ (0.16) and $K_{\mathbf{MC4}^{2+}}/K_{\mathbf{MV}^{2+}}$ (0.24) ratios are close to the statistical value of 0.25.[68] At the higher concentrations that were used for ^{1}H NMR (Fig. S12 and S13 in the ESI†) and the higher **CB[7]**/**MC3**$^{2+}$ or **CB[7]**/**MC4**$^{2+}$ host–guest ratios employed for ESI-MS measurements (Fig. S8 and S9 in the ESI†), other host–guest complexes were observed, namely the [3]pseudorotaxanes, **MC3**$^{2+}\subset$**(CB[7])**$_2$ and **MC4**$^{2+}\subset$**(CB[7])**$_2$. For these complexes, the ^{1}H NMR titrations suggested that the second **CB[7]**

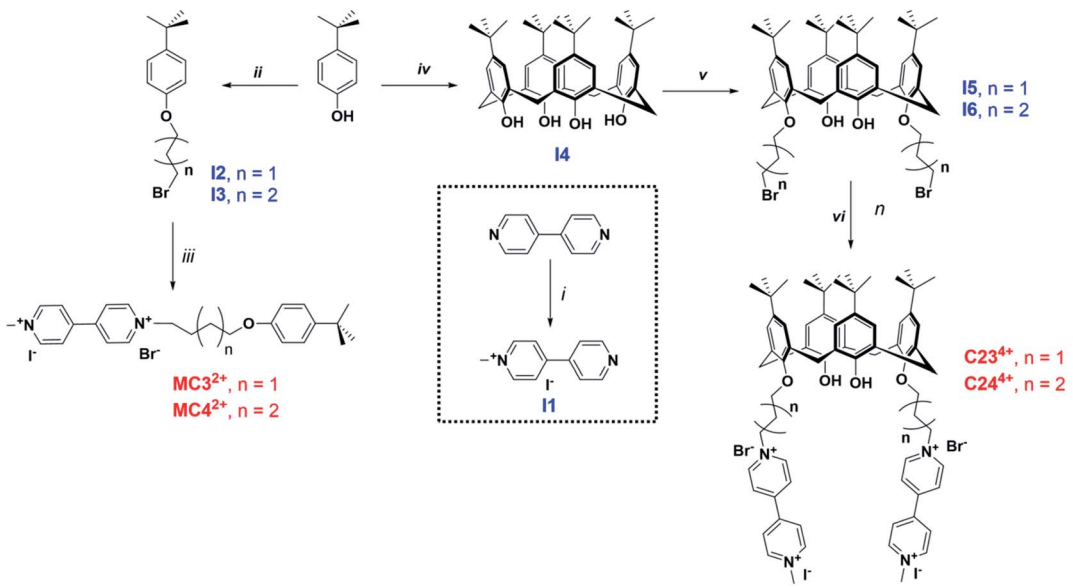

Scheme 1 Synthetic route to the MC3^{2+} and MC4^{2+} monomers as well as the calix[4]arene-bis-viologen systems C23^{4+} and C24^{4+}. Conditions: (i) CH_3I, acetone, reflux, 24 h, 63%; (ii) **I2**: 1,3-dibromopropane, K_2CO_3, acetone, reflux, 48 h, yield 70%; **I3**: 1,4-dibromobutane, K_2CO_3, acetone, reflux, 72 h, yield 27%; (iii) MC3^{2+}: **I1**, CH_3CN, reflux, 72 h, 31%; MC4^{2+}: **I1**, CH_3CN, reflux, 72 h, 71%; (iv) NaOH, HCHO, 100 °C, then heating at 195–250 °C in diphenyl ether, toluene, xylene, yield 63%; (v) **I5**: 1,3-dibromopropane, K_2CO_3, acetone, reflux, 96 h, yield 92%; **I6**: 1,4-dibromobutane, K_2CO_3, acetone, reflux, 96 h, yield 65%; (vi) (iii) C23^{4+}: **I1**, CH_3CN, reflux, 72 h, 85%; C24^{4+}: **I1**, CH_3CN, reflux, 72 h, 67%.

© 2021 The Author(s). Published by the Royal Society of Chemistry

Open Access Article. Published on 02 September 2021. Downloaded on 4/18/2026 12:09:39 PM.
This article is licensed under a Creative Commons Attribution-NonCommercial 3.0 Unported Licence.

Table 1 Thermodynamic and spectroscopic parameters of [*n*]pseudorotaxanes formed with **CB[7]**[a]

		V	**V⊂CB[7]**
Viologen **V**	log $K_{V\subset CB[7]}$	λ (ε) nm (10^4 M^{-1} cm^{-1})	λ (ε) nm (10^4 M^{-1} cm^{-1})
MV^{2+}	5.30 (2)	227 (2.96)/257 (2.06)	226 (3.13)/281 (sh)
MC3^{2+}	4.51 (6)	224 (2.29)/259 (2.17)	223 (2.49)/255 (1.51)
MC4^{2+}	4.68 (5)	224 (2.17)/260 (2.29)	224 (2.48)/252 (1.40)
C23^{4+}	4.5 (1)	224 (7.42)/262 (3.20)	225 (7.50)/275 (2.10)
C24^{4+}	4.44 (8)	220 (7.16)/263 (2.99)	220 (7.29)/280 (1.83)

[a] Solvent: water buffered at pH 7.0 with 0.1 M $Na_2H_2PO_4/NaH_2PO_4$); l = 1 cm; T = 25.0(1) °C. The error (indicated in brackets) on the stability constants correspond to 3σ with σ = standard deviation. sh = shoulder.

macrocycle is sitting in close proximity to the *tert*-butyl-phenyl unit (Fig. 2a). Binding of the first **CB[7]** indeed mainly affects the β and β′ protons of the **BIPY**$^{2+}$ unit, while recognition of the second **CB[7]** macrocycle influences the protons of the *tert*-butyl-phenyl residue (Fig. S12 and S13 in the ESI†). The inability to quantify the second recognition event leading to the formation of **MC3**$^{2+}\subset$**(CB[7])**$_2$ or **MC4**$^{2+}\subset$**(CB[7])**$_2$ by absorption spectrophotometry likely resulted from weak spectral variations and their much lower stability constants.

To gain further insight into the molecular recognition properties, diffusion coefficients were determined by ^{1}H NMR-DOSY for **MC3**$^{2+}$ and **MC4**$^{2+}$ both in the absence and in the presence of increasing amounts of **CB[7]** (Table 2). Firstly, a comparison of the diffusion coefficients of the free **MC3**$^{2+}$ and **MC4**$^{2+}$ revealed similar values, which indicated that both model systems share common structural properties (*i.e.*, comparable volume of 303 cm^3 mol^{-1} for **MC3**$^{2+}$ and 318 cm^3 mol^{-1} for **MC4**$^{2+}$ estimated with DFT) notwithstanding the slightly elongated carbon spacer for **MC4**$^{2+}$. Secondly, the values of the diffusion coefficients decreased as a function of the number of equivalents of **CB[7]**, demonstrating the successive formation of host–guest species of increasing volume and weight (*e.g.*, volume of 928 cm^3 mol^{-1} obtained with DFT for **MC3**$^{2+}\subset$**CB[7]**). Lastly, the diffusion coefficients measured for **MC3**$^{2+}$ and **MC4**$^{2+}$ using the same amount of **CB[7]** are comparable to one another, which suggested that the [2]pseudorotaxanes, **MC3**$^{2+}\subset$**CB[7]** and **MC4**$^{2+}\subset$**CB[7]**, and the [3]pseudorotaxanes, **MC3**$^{2+}\subset$**(CB[7])**$_2$ and **MC4**$^{2+}\subset$**(CB[7])**$_2$, are roughly structurally equivalent. The inability to determine the stability constant of [3]pseudorotaxane prevents the evaluation of the diffusion coefficients specific to each inclusion complex (*i.e.*, [2]- and [3]pseudorotaxanes).

Recognition of C23^{4+} **and C24**$^{4+}$ **by CB[7].** Altogether, absorption binding titrations (Fig. S6 and S7 in the ESI†), ^{1}H-NMR data (Fig. S14 and S15 in the ESI†), and ESI-MS experiments (Fig. S10 and S11 in the ESI†) demonstrated that the [3]pseudorotaxanes, **C23**$^{4+}\subset$**(CB[7])**$_2$ and **C24**$^{4+}\subset$**(CB[7])**$_2$, formed predominantly. Hypochromic and bathochromic shifts of the absorption bands which correspond to the π–π* transitions of the **BIPY**$^{2+}$ cores were observed in both cases (Table 1) as a consequence of the encapsulation of the terminal **BIPY**$^{2+}$ chromophores within the hydrophobic macrocyclic cavity of **CB[7]**. The absorption bands which correspond to the π–π* transitions for the calix[4]arene core remained unaffected by **CB[7]** complexation. As previously shown with the model systems, **MC3**$^{2+}$ and **MC4**$^{2+}$, the presence of a hydrophobic alkoxy substituent did not alter the molecular recognition properties. As a result, the two **CB[7]** macrocycles remained bound to the middle of each of the two **BIPY**$^{2+}$ terminal electrophores as evidenced by ^{1}H NMR spectroscopy (Fig. S14 and S15 in the ESI†). The apparent stability constants (log $K^*_{\mathbf{CB23^{4+}\subset(CB[7])_2}}$ = 4.5(1) and log $K^*_{\mathbf{CB24^{4+}\subset(CB[7])_2}}$ = 4.44(8)) were found to be close

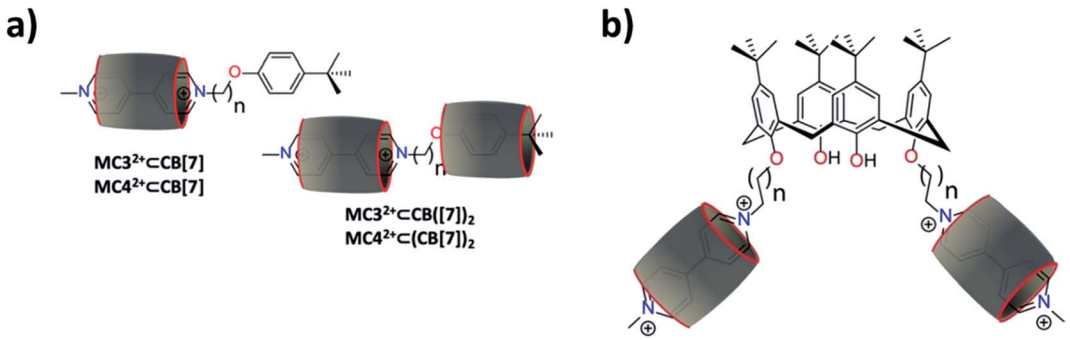

Fig. 2 Schematic representation of (a) the [2]pseudorotaxanes **MC3**$^{2+}\subset$**CB[7]** and **MC4**$^{2+}\subset$**CB[7]** (**CB[7]** mainly resides on the bipyridinium group) and of **MC3**$^{2+}\subset$**(CB[7])**$_2$ and **MC4**$^{2+}\subset$**(CB[7])**$_2$ (*i.e.*, the hydrophobic cavity of the second **CB[7]** is sitting close to the terminal phenyl group); and (b) the [3]pseudorotaxanes **C23**$^{4+}\subset$**(CB[7])**$_2$ and **C24**$^{4+}\subset$**(CB[7])**$_2$ (*i.e.*, the **CB[7]** mainly resides on the bipyridinium groups). n = 2, or 3. **CB[7]** is represented with the grey cylinder.

© 2021 The Author(s). Published by the Royal Society of Chemistry

Open Access Article. Published on 02 September 2021. Downloaded on 4/18/2026 12:09:39 PM. This article is licensed under a Creative Commons Attribution-NonCommercial 3.0 Unported Licence.

Table 2 Diffusion coefficients of $MC3^{2+}$, $MC4^{2+}$, $C23^{4+}$ and $C24^{4+}$ in the absence and the presence of CB[7] [a]

D ($\times 10^{-6}$ cm^2 s^{-1})									
No CB[7]		+1 eq. CB[7]		+2 eq. CB[7]		No CB[7]		+2 eq. CB[7]	
$MC3^{2+}$	$MC4^{2+}$	$MC3^{2+}$	$MC4^{2+}$	$MC3^{2+}$	$MC4^{2+}$	$C23^{4+}$	$C24^{4+}$	$C23^{4+}$	$C24^{4+}$
6.51	6.57	4.89	4.17	3.56	3.29	2.58	4.30	3.85	3.11

[a] Measured by DOSY experiments on a 600 MHz spectrometer, D_2O, 298 K. The errors on these values are estimated to less than 5%.

to those evaluated for the corresponding models, $MC3^{2+}$ and $MC4^{2+}$ (Table 1). Again, these stability constant values were found to be lower than those measured for MV^{2+} (log $K_{MV^{2+}\subset CB[7]} = 5.30(2)$) as a consequence of the presence of the bulky calix[4]arene core (Fig. 2b).

Diffusion coefficients were also determined for $C23^{4+}$ and $C24^{4+}$ both in the absence and the presence of CB[7]. In contrast to the values measured for the model ligands, the D value measured for $C23^{4+}$ was found to be lower than that of $C24^{4+}$. One would expect that the extended spacer of $C24^{4+}$ should increase the global volume of the molecule (*i.e.*, DFT calculated volumes of 824 cm^3 mol^{-1} for $C23^{4+}$ and 873 cm^3 mol^{-1} for $C24^{4+}$), thereby causing it to diffuse slower in solution. This unexpected result thus might be explained by the slightly more flexible arms of $C24^{4+}$ which should minimize the steric interactions of the viologen units with the bulky calix[4]arene core, thereby resulting in markedly different solvation properties with respect to $C23^{4+}$. As a consequence, the diffusion coefficient decreases in the presence of CB[7] for $C24^{4+}$, while it increases for $C23^{4+}$, so that both converge to a comparable value, the volumes of host–guest species with $C23^{4+}$ and $C24^{4+}$ being then globally equivalent in the presence of CB[7].

Characterization of the radical cations

Intermolecular *versus* intramolecular dimerization of the radical cations. We have demonstrated that $MC3^{\bullet+}$ and $MC4^{\bullet+}$ rapidly pimerize (Fig. S21 and S22 in the ESI†) in aqueous solution with a log K_{Dim} value of 3.4. This value is very similar to the value previously determined for the benzyl methyl viologen radical cation $BMV^{\bullet+}$ (log $K_{Dim} = 3.46(5)$),[30] but much higher than that reported for the methyl viologen radical cation $MV^{\bullet+}$ (log K_{Dim} ~2.5–2.9).[69,70] The values of K_{Dim} are also similar to those measured for viologens decorated with hydrophobic alkyl substituents.[15] This suggested that increasing the hydrophobicity around the $BIPY^{\bullet+}$ unit with aryl/alkyl substituents favors the intermolecular pimerization in aqueous solution. Moreover, we could again demonstrate that the extended spacer for $MC4^{\bullet+}$ does not drastically alter its pimerization since similar K_{Dim} values were calculated for $MC3^{\bullet+}$ and $MC4^{\bullet+}$. These two radical cations are characterized by intense and structured absorption bands in the visible region ($MC3^{\bullet+}$: λ_{max} ~602 nm, $\varepsilon^{602} = 1.01 \times 10^4$ M^{-1} cm^{-1}; $MC4^{\bullet+}$: λ_{max} ~602 nm, $\varepsilon^{602} = 9.56 \times 10^3$ M^{-1} cm^{-1}, Fig. S21 and S22 in the ESI†), in agreement with the spectroscopic parameters determined for $MV^{\bullet+}$ (600–606 nm)[15,23,67,71] and $BMV^{\bullet+}$ (600 nm).[30] Formation of the radical cation dimers induced a significant hypsochromic shift of the absorption band at ~600 nm ($\Delta\lambda$ ~50 nm) and gave rise to intense absorption bands corresponding to radical–radical transitions in the NIR region (λ_{max} > 850–900 nm).[15] These UV-vis absorption studies also demonstrated that no significant pimerization occurs unless the concentration of the radical cations is high enough (>10^{-3} M, Fig. S21 and S22 in the ESI†). As previously reported,[31–45] preorganization of the $BIPY^{2+}$ electrophores to within close proximity of one another around a robust and inert molecular platform can enhance their pimerization, leading to very stable π-dimers in aqueous solution.

Upon chemical generation of the radical cations, $C23^{2(\bullet+)}$ and $C24^{2(\bullet+)}$ (Fig. S27 and S28 in the ESI†), intense absorption bands appeared at ~530 nm (Fig. 3). An additional intense absorption band centered at 1072 nm for $C23^{2(\bullet+)}$ and at 925 nm for $C24^{2(\bullet+)}$ were observed and are unambiguously assigned to the intramolecular charge resonance that occurs in the dimerized viologen radical cation species. This feature indicated that a two-electron reduction of $C23^{4+}$ and $C24^{4+}$ leads to two radical divalent cations, $C23^{2(\bullet+)}$ and $C24^{2(\bullet+)}$, that spontaneously pimerize intramolecularly, leading to a stable radical dimeric species.

The NIR absorption spectroscopic signatures of the π-dimerized complexes were demonstrated to be closely related to the extent of overlapping between both π-orbitals of the $BIPY^{\bullet+}$ radicals.[45] When a propyloxy chain links the viologens to the calix[4]arene moiety ($C23^{2(\bullet+)}$: λ_{max} ~960 nm in CH_3CN[45] and λ_{max} ~1070 nm in water), DFT calculations at the BLYP-D3/

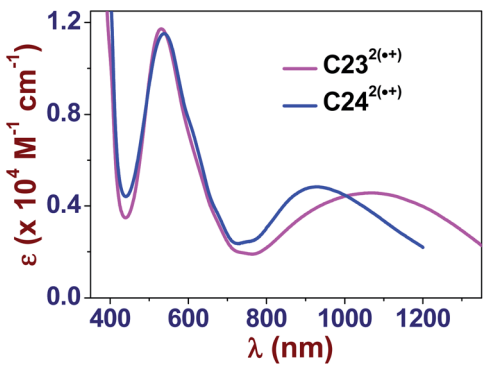

Fig. 3 Electronic UV-vis-NIR absorption spectra of $C23^{2(\bullet+)}$ and $C24^{2(\bullet+)}$ in water. Solvent: water buffered at pH 7.0 with 0.1 M Na_2HPO_4/NaH_2PO_4. T = 25.0(1) °C.

© 2021 The Author(s). Published by the Royal Society of Chemistry

Open Access Article. Published on 02 September 2021. Downloaded on 4/18/2026 12:09:39 PM.
This article is licensed under a Creative Commons Attribution-NonCommercial 3.0 Unported Licence.

DZVP level suggested that only one pyridinium ring per viologen radical is involved in the intramolecular π-dimerization process. This result, which is imposed by geometric constraints that is inherent to the length and structure of the propyl chain, is not observed with the ethyloxy-derived calix[4]arene-bis-viologen ($\mathbf{C22^{2(\bullet+)}}$: λ_{max} ~860 nm in CH_3CN[45]), which affords a fully face-to-face stacked arrangement. DFT calculations performed at the M06-2X/6-311G(d,p) level (Fig. 4) provided a minimum energy conformation for $\mathbf{C22^{2(\bullet+)}}$ in which the two $\mathbf{BIPY^{\bullet+}}$ units display an almost perfect face-to-face interaction. Similarly, the $\mathbf{BIPY^{\bullet+}}$ units in $\mathbf{C23^{2(\bullet+)}}$ are twisted with respect to each other by an angle of ~78°, reducing the overlap between the corresponding π-orbitals. Increasing the length from 3 to 4 carbons (butyloxy derivative, $\mathbf{C24^{2(\bullet+)}}$: λ_{max} ~925 nm in water) does not completely reinstate the face-to-face dimerized π-stacking orientation, but it does increase the overlap of the π-orbitals with respect to $\mathbf{C23^{2(\bullet+)}}$ with a twist angle of ~60°. Thus, the nature and size of the linker between the calix[4]arene platform and the terminal $\mathbf{BIPY^{\bullet+}}$ radical cations, as well as the nature of the platform, with the calix[4]arene displaying a cone conformation, appear to be crucial factors that govern the arrangement of the π-dimers. It is noteworthy that preorganization of the designed systems apparently allows for efficient intramolecular dimerization of the two viologens upon reduction in a range of solvents (*e.g.*, water and CH_3CN[45]).

Reduction of the [*n*]pseudorotaxanes with CB[7]

Monocationic monoradicals $\mathbf{MC3^{\bullet+}}$ and $\mathbf{MC4^{\bullet+}}$. Cyclic voltammetry (Fig. S16 in the ESI†), square-wave voltammetry (Fig. 5), and EPR (Fig. S17 and S18 in the ESI†) measurements in phosphate-buffered solutions at pH 7 were performed on the model systems, $\mathbf{MC3^{2+}}$ and $\mathbf{MC4^{2+}}$, in the absence and presence of **CB[7]**. Both systems were characterized by two successive one-electron reversible redox waves: $E_{1/2}1$ ($\mathbf{MC3^{2+}} \rightarrow \mathbf{MC3^{\bullet+}}$) = −0.56 V and $E_{1/2}2$ ($\mathbf{MC3^{\bullet+}} \rightarrow \mathbf{MC3^{0}}$) = −0.83 V; $E_{1/2}{}^{1}$ ($\mathbf{MC4^{2+}} \rightarrow \mathbf{MC4^{\bullet+}}$) = −0.56 V and $E_{1/2}{}^{2}$ = −0.83 V. In the presence of three equivalents of **CB[7]**, where it is assumed that $\mathbf{MC3^{2+}}\subset\mathbf{CB[7]}$ and $\mathbf{MC4^{2+}}\subset\mathbf{CB[7]}$ predominate, both redox waves shifted slightly to more negative potentials (Table 3) while retaining their reversible shapes.

These shifts corresponded to the signatures of the relative affinities of **CB[7]** for the different redox states of the model systems. Assuming a $\log K_{\mathbf{MC3^{2+}}\subset\mathbf{CB[7]}}$ value of 4.51(6) for $\mathbf{MC3^{2+}}\subset\mathbf{CB[7]}$ (Fig. S1 in the ESI†), a $\log K_{\mathbf{MC3^{\bullet+}}\subset\mathbf{CB[7]}}$ of ~4–4.2

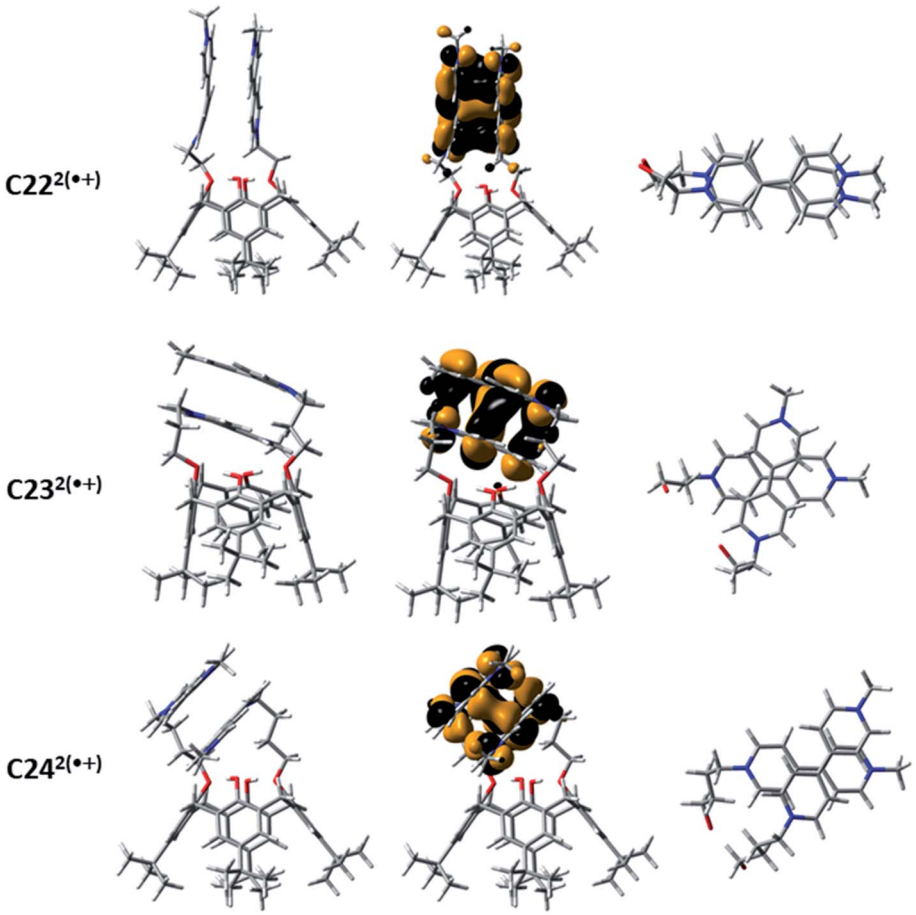

Fig. 4 Geometries obtained with DFT (M062X/6-311G(d,p)) (left panel), the corresponding HOMOs (central panel) and detail of the arrangements of the redox-active $\mathbf{BIPY^{\bullet+}}$ units within the two electrons reduced calix[4]arene-bis-viologens $\mathbf{C22^{2(\bullet+)}}$, $\mathbf{C23^{2(\bullet+)}}$ and $\mathbf{C24^{2(\bullet+)}}$ that undergo intramolecular pimerization.

Open Access Article. Published on 02 September 2021. Downloaded on 4/18/2026 12:09:39 PM.
This article is licensed under a Creative Commons Attribution-NonCommercial 3.0 Unported Licence.

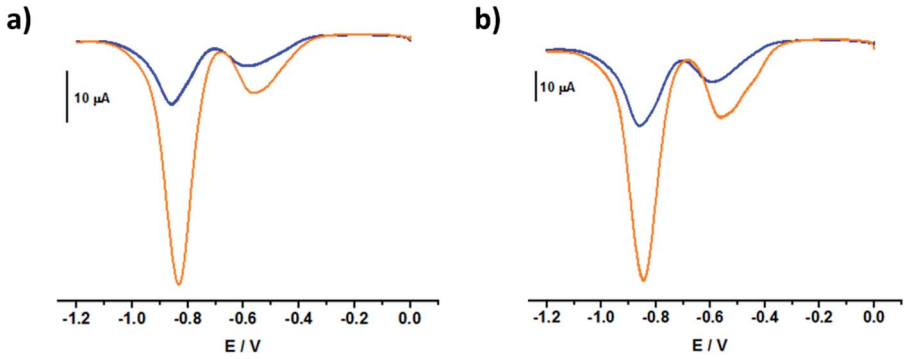

Fig. 5 Square wave voltammograms of (a) $MC3^{2+}$, [$MC3^{2+}$] = 0.05 mM and b) $MC4^{2+}$, [$MC4^{2+}$] = 0.06 mM in the absence (orange) and the presence of **CB[7]** (blue, 3 equivalents of **CB[7]**). All voltammograms were recorded in argon-purged phosphate buffer solutions (pH 7) at 298 K (*E versus* Ag/AgCl).

Table 3 Values of $E_{1/2}$ (in V) for $MC3^{2+}$ (0.05 mM), $MC4^{2+}$ (0.063 mM), $C23^{4+}$ (0.05 mM) and $C24^{4+}$ (0.05 mM) measured by cyclic voltammetry (CV) and square wave voltammetry (SWV) in the absence and in the presence of 3 equivalents of **CB[7]** for $MC3^{2+}$, $MC4^{2+}$ and $C23^{4+}$, and 4 equivalents of **CB[7]** for$C24^{4+}$

Species	$E_{1/2}{}^1$ (CV)	$E_{1/2}{}^1$ (SW)	$E_{1/2}{}^2$ (CV)	$E_{1/2}{}^2$ (SW)
$MC3^{2+}$	−0.56 V	−0.56 V	−0.83 V	−0.83 V
$MC3^{2+}$ + 3 eq. **CB[7]**	−0.60 V	−0.59 V	−0.85 V	−0.86 V
$MC4^{2+}$	−0.56 V	−0.56 V	−0.83 V	−0.84 V
$MC4^{2+}$ + 3 eq. **CB[7]**	−0.58 V	−0.58 V	−0.83 V	−0.86 V
$C23^{4+}$	−0.42 V	−0.43 V	−0.84 V	−0.85 V
$C23^{4+}$ + 3 eq. **CB[7]**	−0.44 V	−0.46 V	−0.84 V	−0.85 V
$C24^{4+}$	−0.45 V	−0.47 V	−0.85	−0.85
$C24^{4+}$ + 4 eq. **CB[7]**	−0.50	−0.51	−0.85	−0.85

and a $\log K_{\mathbf{MC3^{(0)}\subset CB[7]}}$ of ∼3.5–3.9 values were accordingly calculated.[26,29] Similarly, using a $\log K_{\mathbf{MC4^{2+}\subset CB[7]}}$ value of 4.68(5) (Fig. S3 in the ESI†), a $\log K_{\mathbf{MC4^{\bullet+}\subset CB[7]}}$ of ∼4.2 and a $\log K_{\mathbf{MC4^{0}\subset CB[7]}}$ of ∼3.8 were calculated. Using an electrochemical approach, these calculated values were in reasonably good agreement, within error, with those derived from direct absorption binding titrations ($\log K_{\mathbf{MC3^{\bullet+}\subset CB[7]}} = 3.8(4)$ (Fig. S24 in the ESI†) and $\log K_{\mathbf{MC4^{\bullet+}\subset CB[7]}} = 4.54(5)$ (Fig. S26 in the ESI†). In contrast to $\mathbf{BMV^{2+}}$, where translational motion of the **CB[7]** macrocycle occurred upon electrochemical reduction of the bipyridinium unit,[30] the **CB[7]** macrocycle remained firmly bound to the $\mathbf{BIPY^{2+}}$ electroactive units of the $\mathbf{MC^{4+}}$ derivatives regardless of their oxidation state.

Assuming that only the first one-electron reduction process dominates from 0 V to −0.7 V (Fig. S16 in the ESI† and Fig. 5), the diffusion coefficients of $\mathbf{MC3^{2+}}$ and $\mathbf{MC4^{2+}}$ in the absence and in the presence of **CB[7]** (Table 4) can be evaluated by chronocoulometric experiments. The differences observed between the values of the diffusion coefficients of $\mathbf{MC3^{\bullet+}}$/$\mathbf{MC3^{2+}}$ and $\mathbf{MC4^{\bullet+}}$/$\mathbf{MC4^{2+}}$ could be an indication of the dimerization of the model systems upon the one -electron reduction reactions. Addition of **CB[7]** suppresses the pimerization process in favor of the inclusion complexes. As a consequence, the inclusion complexes with **CB[7]** have lower diffusion coefficients than the corresponding free viologens.

Investigations of the UV-vis-NIR absorption spectra of $\mathbf{MC3^{2+}}$ and $\mathbf{MC4^{2+}}$ in water at pH 7.0 in the absence or in the presence of a reducing agent were carried out to evaluate the effect of **CB[7]** addition (Fig. S23 and S25 in the ESI†). $\mathbf{MC3^{\bullet+}\subset CB[7]}$ and $\mathbf{MC4^{\bullet+}\subset CB[7]}$ both clearly exhibited a significant hypochromic shift of the visible absorption band associated with the radical cation with increasing concentration of **CB[7]**, strong evidence for the inclusion of the $\mathbf{BIPY^{\bullet+}}$ radical cation within the hydrophobic cavity of **CB[7]**. This binding event effectively hampers radical cation pimerization.

Bisradicals $\mathbf{C23^{2(\bullet+)}}$ and $\mathbf{C24^{2(\bullet+)}}$. Cyclic (Fig. S16 in the ESI†) and square wave (Fig. 6) voltammetry studies were undertaken to evaluate the impact of **CB[7]** addition on the intramolecular pimerization of the $\mathbf{BIPY^{\bullet+}}$ radical cations of the calix[4]arene-bis-viologens, $\mathbf{C23^{4+}}$ and $\mathbf{C24^{4+}}$. The electrochemical data clearly showed two distinct and reversible redox waves. The relative amplitudes and shapes of the peaks for each wave at the anode (oxidation) are similar to those observed at the cathode (reduction). Such a pattern is an indication of the redox reversibility of the system.

Table 4 Diffusion coefficients D ($cm^2\ s^{-1}$) of $MC3^{2+}$, $MC4^{2+}$, $C23^{4+}$ and $C24^{4+}$ measured by chronocoulometry in H_2O (0.1 M TBACl) in the absence and the presence of **CB[7]**. The errors on these values are 10%

No **CB[7]**/D	+**CB[7]**/D
$\mathbf{MC3^{\bullet+}}/0.7 \times 10^{-5}$	$\mathbf{MC3^{\bullet+}}$ + 2 eq. **CB[7]**/1.9×10^{-5}
$\mathbf{MC3^{2+}}/5.4 \times 10^{-5}$	$\mathbf{MC3^{2}}$ + 2 eq. **CB[7]**/14.2×10^{-5}
$\mathbf{MC4^{\bullet+}}/3.1 \times 10^{-5}$	$\mathbf{MC4^{\bullet+}}$ + 2 eq. **CB[7]**/6.2×10^{-5}
$\mathbf{MC4^{2+}}/81.0 \times 10^{-5}$	$\mathbf{MC4^{2+}}$ + 2 eq. **CB[7]**/22×10^{-5}
$\mathbf{C23^{\bullet+}}/1.41 \times 10^{-5}$	$\mathbf{C23^{\bullet+}}$ + 3 eq. **CB[7]**/2.9×10^{-5}
$\mathbf{C23^{2+}}/7.58 \times 10^{-5}$	$\mathbf{C23^{2}}$ + 3 eq. **CB[7]**/3.91×10^{-5}
$\mathbf{C24^{\bullet+}}/0.81 \times 10^{-5}$	$\mathbf{C24^{\bullet+}}$ + 4 eq. **CB[7]**/0.16×10^{-5}
$\mathbf{C24^{2+}}/20.1 \times 10^{-5}$	$\mathbf{C24^{2+}}$ + 4 eq.**CB[7]**/42.1×10^{-5}
$\mathbf{C23^{\bullet+}}/1.41 \times 10^{-5}$	$\mathbf{C23^{\bullet+}}$ + 3 eq. **CB[7]**/2.9×10^{-5}
$\mathbf{C23^{2+}}/7.58 \times 10^{-5}$	$\mathbf{C23^{2}}$ + 3 eq. **CB[7]**/3.91×10^{-5}
$\mathbf{C24^{\bullet+}}/0.81 \times 10^{-5}$	$\mathbf{C24^{\bullet+}}$ + 4 eq. **CB[7]**/0.16×10^{-5}
$\mathbf{C24^{2+}}/20.1 \times 10^{-5}$	$\mathbf{C24^{2+}}$ + 4 eq. **CB[7]**/42.1×10^{-5}

© 2021 The Author(s). Published by the Royal Society of Chemistry

Open Access Article. Published on 02 September 2021. Downloaded on 4/18/2026 12:09:39 PM.
This article is licensed under a Creative Commons Attribution-NonCommercial 3.0 Unported Licence.

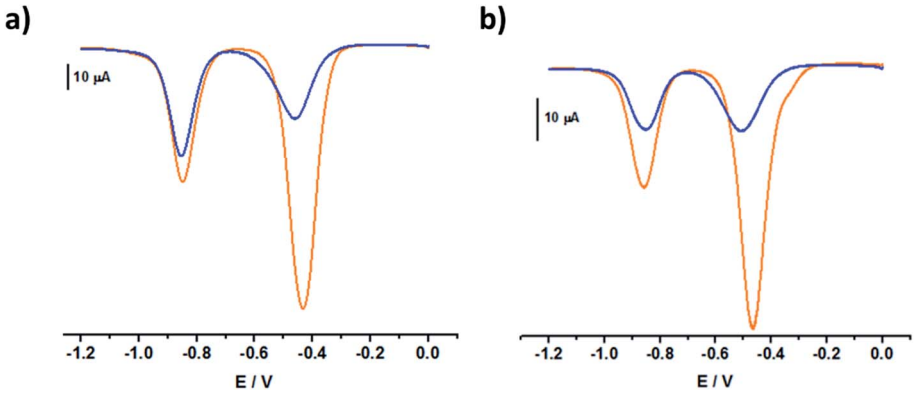

Fig. 6 Square wave voltammograms of (a) $C23^{4+}$, [$C23^{4+}$] = 0.05 mM and (b) $C24^{4+}$, [$C24^{4+}$] = 0.05 mM in the absence (orange line) and the presence of CB[7] (blue line, respectively 3 and 4 equivalents of CB[7]). All voltammograms were recorded in argon-purged phosphate buffer solutions (pH 7) at 298 K (*E versus* Ag/AgCl).

The square wave voltammograms of $\mathbf{C23^{4+}}$ and $\mathbf{C24^{4+}}$ (Fig. 6) displayed two reversible two-electron reduction processes: $E^{1}{}_{1/2}$ ($\mathbf{C23^{4+}} \rightarrow \mathbf{C23^{2(\cdot+)}}$) = −0.43 V and $E_{1/2}{}^{2}$ ($\mathbf{C23^{2(\cdot+)}} \rightarrow \mathbf{C23^{0}}$) = −0.85 V; $E_{1/2}{}^{1}$ ($\mathbf{C24^{4+}} \rightarrow \mathbf{C24^{2(\cdot+)}}$) = −0.47 V and $E_{1/2}{}^{2}$ ($\mathbf{C24^{2(\cdot+)}} \rightarrow \mathbf{C24^{0}}$) = −0.85 V. Interestingly, for the [3]pseudorotaxanes, $\mathbf{C23^{4+}}\subset\mathbf{(CB[7])_2}$ and $\mathbf{C24^{4+}}\subset\mathbf{(CB[7])_2}$, no shifts were observed for the second reduction wave (Table 3), which would have corresponded to the following electrochemical processes: $\mathbf{C23^{2(\cdot+)}}\subset\mathbf{(CB[7])_2} \rightarrow \mathbf{C23^{0}}\subset\mathbf{(CB[7])_2}$ and $\mathbf{C24^{2(\cdot+)}}\subset\mathbf{(CB[7])_2} \rightarrow \mathbf{C24^{0}}\subset\mathbf{(CB[7])_2}$. Rather, our observations indicated that after the first two-electron reduction process, the threads behave as if they are unbound $\mathbf{C23^{2(\cdot+)}}$ and $\mathbf{C24^{2(\cdot+)}}$. In other words, the first reduction of $\mathbf{C23^{4+}}\subset\mathbf{(CB[7])_2}$ and $\mathbf{C24^{4+}}\subset\mathbf{(CB[7])_2}$ induced dethreading of the **CB[7]** macrocycles, which is spontaneously followed by intramolecular dimerization of the two terminal $\mathbf{BIPY^{\cdot+}}$ groups, leading to the formation of intramolecular dimeric species, $\mathbf{C23^{2(\cdot+)}}$ and $\mathbf{C24^{2(\cdot+)}}$. These results were consistent with the absorption spectrophotometric analyses (Fig. S27 and S28 in the ESI†) and EPR behavior (Fig. S19 and S20 in the ESI†) of the $\mathbf{C23^{4+}}$/**CB[7]** and $\mathbf{C24^{4+}}$/**CB[7]** [3]pseudorotaxanes.

Chronocoulometry was also used to evaluate the diffusion coefficients of the fully oxidized and radical cationic states of the different species in aqueous solution. During the two electrons reduction process (0 V → −0.7 V) the fully oxidized species predominate and diffuse to the electrode surface where they are reduced. By measuring the reduction rates, the diffusion constants for $\mathbf{C23^{4+}}$ and $\mathbf{C24^{4+}}$ species can be calculated in the absence and in the presence of **CB[7]** (Table 4). Alternatively, by setting the voltage to −0.7 V and performing the oxidation process, the rates of oxidation and the diffusion coefficients of the corresponding radical cationic species can be measured as well. In the absence of **CB[7]**, larger diffusion coefficients were observed for $\mathbf{C23^{4+}}$ and $\mathbf{C24^{4+}}$ than for their corresponding fully reduced forms. This could be explained by the ability of higher charged species to diffuse faster towards or away from an electrode. In the presence of **CB[7]**, larger diffusion coefficients were measured for the [3]pseudorotaxanes $\mathbf{C23^{4+}}\subset\mathbf{(CB[7])_2}$ and $\mathbf{C23^{4+}}\subset\mathbf{(CB[7])_2}$ than the corresponding reduced species (*i.e.*, upon reduction, a dethreading of the **CB[7]** occurs as a consequence of favored intramolecular pimerization with respect to the recognition process). Here also, one would expect that the [3]pseudorotaxanes $\mathbf{C23^{4+}}\subset\mathbf{(CB[7])_2}$ and $\mathbf{C23^{4+}}\subset\mathbf{(CB[7])_2}$ display larger hydrodynamic size by comparison with $\mathbf{C23^{2(\cdot+)}}$ or $\mathbf{C24^{2(\cdot+)}}$. Markedly different solvation of the latter species is suggested to explain these peculiar properties. The close diffusion coefficients of the radical cation species in the absence and the presence of **CB[7]** indicate that the dimerization of the viologen radical cations induce a dethreading of the **CB[7]** macrocycles.

Recognition of the viologen derivatives by CB[8]. The characterization of the host–guest complexes formed between $\mathbf{MC3^{2+}}$, $\mathbf{MC4^{2+}}$, $\mathbf{C23^{4+}}$, and $\mathbf{C24^{4+}}$ with **CB[8]** was investigated by absorption spectrophotometry (Fig. S29 to S32 in the ESI†) and ESI-MS measurements (Fig. 7). Due to the limited solubility of **CB[8]**, we were not able to perform ^{1}H NMR titrations of the corresponding viologens. Similarly to the [*n*]pseudorotaxanes formed with **CB[7]**, we were able to observe evidence for the formation of [2]pseudorotaxanes with $\mathbf{MC3^{2+}}$ and $\mathbf{MC4^{2+}}$ (namely $\mathbf{MC3^{2+}}\subset\mathbf{CB[8]}$ and $\mathbf{MC4^{2+}}\subset\mathbf{CB[8]}$) and [3]pseudorotaxanes with $\mathbf{C23^{4+}}$ and $\mathbf{C24^{4+}}$ (namely a $\mathbf{C23^{4+}}\subset\mathbf{(CB[8])_2}$ and $\mathbf{C24^{4+}}\subset\mathbf{(CB[8])_2}$).

For the latter [3]pseudorotaxanes, chemical reduction of the $\mathbf{BIPY^{2+}}$ electroactive units led to dethreading of the **CB[8]** macrocyclic host despite its larger cavity size (Fig. S31 and S32 in the ESI†). This suggests significant steric constraints with the calix[4]arene platform and/or poor flexibility of the designed systems even though longer and apparently more flexible spacers were introduced. However, the $\mathbf{MC3^{2+}}$ and $\mathbf{MC4^{2+}}$ models clearly led (Fig. S29 and S30 in the ESI†) to the expected [3]pseudorotaxanes $\mathbf{(MC3^{\cdot+})_2}\subset\mathbf{CB[8]}$ and $\mathbf{(MC4^{\cdot+})_2}\subset\mathbf{CB[8]}$ thus emphasizing the detrimental role of the anchoring platform rather than the length of the spacers. The occurrence of [3]pseudorotaxanes $\mathbf{(MC3^{\cdot+})_2}\subset\mathbf{CB[8]}$ and $\mathbf{(MC4^{\cdot+})_2}\subset\mathbf{CB[8]}$ upon reduction is in agreement with the published reports[26–28] that showed that the stability of methyl viologen dimer $\mathbf{(MV^{\cdot+})_2}\subset\mathbf{CB[8]}$ was significantly increased in the presence of **CB[8]**

Open Access Article. Published on 02 September 2021. Downloaded on 4/18/2026 12:09:39 PM.
This article is licensed under a Creative Commons Attribution-NonCommercial 3.0 Unported Licence.

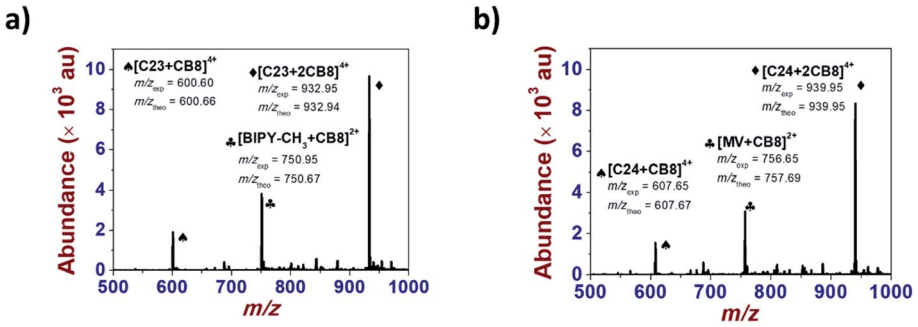

Fig. 7 ESI mass spectra of inclusion complexes of a) $C23^{4+}$ and b) $C24^{4+}$ (bottom) with **CB[8]**. (a) $[C23^{4+}]_0 = 5 \times 10^{-5}$ M; $[CB[7]]_0 = 10^{-4}$ M. Solvent: H_2O; positive mode. $V_c = 200$ V. (b) $[C24^{4+}]_0 = 5 \times 10^{-5}$ M; $[CB[7]]_0 = 10^{-4}$ M. Solvent: H_2O; positive mode. $V_c = 100$ V.

following the formation of a 2 : 1 $(MV^{\bullet+})_2 \subset CB[8]$) supramolecular complex in water.

Conclusions

Two calix[4]arene-bis-viologen systems, namely $C23^{4+}$ and $C24^{4+}$ were synthesized. The host–guest properties were extensively studied using a large set of analytical methods and led to the characterization of [3]pseudorotaxanes in combination with either **CB[7]** or **CB[8]**. For each of these host–guest species, **CB[7]** or **CB[8]** was demonstrated to reside in the middle of the $BIPY^{2+}$ cations as a result of steric interactions with the anchoring platform. Upon reduction of the terminal $BIPY^{2+}$ cations, these [3]pseudorotaxanes spontaneously dissociate as the result of a strong intramolecular dimerization of the two face-to-face viologen radical cations. The arrangement of the $BIPY^{\bullet+}$ radical cations within the dimeric species seemingly relies on the length of the spacer that links the electroactive units to the anchoring moiety. Dethreading and dimerization do not occur in experiments involving **CB[7]** (or **CB[8]**) and either of the two monomeric viologen guests $MC3^{2+}$ and $MC4^{2+}$, which were used a models. On the other hand, the model compounds provided unexpected and valuable properties. Thanks to the presence of a alkoxy-phenyl substitution, [3]pseudorotaxanes such as $MC3^{2+} \subset (CB[7])_2$ and $MC4^{2+} \subset (CB[7])_2$ were characterized. For the $MC3^{2+} \subset CB[7]$ and $MC4^{2+} \subset CB[7]$ [2]pseudorotaxanes, no redox-triggered translocation of **CB[7]** between the two binding stations were observed indicating that the $BIPY^{2+}$ unit remained the favored recognition site whatever its redox state. In the presence of **CB[8]**, similar properties were emphasized with the oxidized form of $MC3^{2+}$ and $MC4^{2+}$ threads. However, [3]pseudorotaxanes $(MC3^{(\bullet+)})_2 \subset CB[8]$ and $(MC4^{(\bullet+)})_2 \subset CB[8]$) were predominantly formed as a consequence of the larger cavity size of the **CB[8]** host. This preliminary study provided interesting information for the further development of functional electroactive systems and will be extended to tetrakis analogues displaying either a cone or 1,3-alternate arrangement of the anchoring calix[4]arene unit.

Conflicts of interest

There are no conflicts to declare.

Acknowledgements

M. E. thank the CNRS (LIMA, UMR 7042) and the University of Strasbourg for funding this research work. C. P.-I. acknowledges Centro de Supercomputación de Galicia (CESGA) for providing access to supercomputing facilities. A. T. thank NYUAD for its generous support of the research program at NYUAD.

Notes and references

1 (*a*) T. Fukino, H. Yamagishi and T. Aida, *Adv. Mater.*, 2016, **29**, 1603888; (*b*) K. Madasamy, D. Velayutham, V. Suryanarayanan, M. Kathiresan and K. C. Ho, *J. Mater. Chem. C*, 2019, **7**, 4622–4637; (*c*) A. F. Greene, M. K. Danielson, A. O. Delawder, K. P. Liles, X. Li, A. Natraj, A. Wellen and J. C. Barnes, *Chem. Mater.*, 2017, **29**, 9498–9508; (*d*) K. C. Ho, H. C. Lu and H. F. Yu, *RSC Smart Mater.*, 2019, **33**, 372–405; (*e*) J. Ding, C. Zheng, L. Wang, C. Lu, B. Zhang, Y. Chen, M. Li, G. Zhai and X. Zhuang, *J. Mater. Chem. A*, 2019, **7**, 23337–23360.

2 K. Wadhwa, S. Nuryyeva, A. C. Fahrenbach, M. Elhabiri, C. Platas-Iglesias and A. Trabolsi, *J. Mater. Chem. C*, 2013, **1**, 2302–2307.

3 (*a*) R. J. Mortimer, *Electrochim. Acta*, 1999, **44**, 2971–2981; (*b*) L. C. Cao, M. Mou and Y. Wang, *J. Mater. Chem.*, 2009, **19**, 3412–3418; (*c*) S. Asaftei, M. Ciobanu, A. M. Lepadatu, E. Song and U. Beginn, *J. Mater. Chem.*, 2012, **22**, 14426–14437.

4 M. Kuroboshi, T. Shiba and H. Tanaka, *Tetrahedron Lett.*, 2013, **54**, 3666–3668.

5 K. Ciepluch, N. Katir, A. El Kadib, A. Felczak, K. Zawadzka, M. Weber, B. Klajnert, K. Lisowska, A. M. Caminade, M. Bousmina, M. Bryszewska and J. P. Majoral, *Mol. Pharmaceutics*, 2012, **9**, 448–457.

6 S. Berger, A. Ghicov, Y. C. Nah and P. Schmuki, *Langmuir*, 2009, **25**, 4841–4844.

7 D. Cummins, G. Boschloo, M. Ryan, D. Corr, S. N. Rao and D. Fitzmaurice, *J. Phys. Chem. B*, 2000, **104**, 11449–11459.

8 G. De Filpo, F. P. Nicoletta and G. Chidichimo, *Chem. Mater.*, 2006, **18**, 4662–4666.

9 R. Cinnsealach, G. Boschloo, S. Nagaraja Rao and D. Fitzmaurice, *Sol. Energy Mater. Sol. Cells*, 1998, **55**, 215–223.

© 2021 The Author(s). Published by the Royal Society of Chemistry

Open Access Article. Published on 02 September 2021. Downloaded on 4/18/2026 12:09:39 PM. This article is licensed under a Creative Commons Attribution-NonCommercial 3.0 Unported Licence.

10 P. Bonhôte, E. Gogniat, M. Grätzel and P. V. Ashrit, *Thin Solid Films*, 1999, **350**, 269–275.
11 P. Sidorov, I. Desta, M. Chessé, D. Horvath, G. Marcou, A. Varnek, E. Davioud-Charvet and M. Elhabiri, *ChemMedChem*, 2016, **11**, 1339–1351.
12 P. M. S. Monk, *The Viologens: Physicochemical Properties, Synthesis and Applications of the Salts of 4, 4'-Bipyridine*, Chichester, 1998.
13 (*a*) J. Bruinink, C. G. A. Kregting and J. J. Ponjeé, *J. Electrochem. Soc.*, 1977, **124**, 1854–1858; (*b*) A. G. Evans, J. C. Evans and M. W. Baker, *J. Am. Chem. Soc.*, 1977, **99**, 5882–5884; (*c*) D. Meisel, W. A. Mulac and M. S. Matheson, *J. Phys. Chem.*, 1981, **85**, 179–187; (*d*) E. Adar, Y. Degani, Z. Goren and I. Willner, *J. Am. Chem. Soc.*, 1986, **108**, 4696–4700; (*e*) A. Yasuda, H. Mori and J. Seto, *J. Appl. Electrochem.*, 1987, **17**, 567–573.
14 (*a*) A. Trabolsi, M. Hmadeh, N. M. Khashab, D. C. Friedman, N. Humbert, M. Elhabiri, H. A. Khatib, M. E. Belowich, A. Coskun, A. M. Albrecht-Gary and J. F. Stoddart, *New J. Chem.*, 2009, **33**, 254–263; (*b*) W. Geuder, S. Hünig and A. Suchy, *Tetrahedron*, 1986, **42**, 1665–1677.
15 E. M. Kosower and J. L. Cotter, *J. Am. Chem. Soc.*, 1964, **86**, 5524–5527.
16 E. M. Kosower and J. Hajdu, *J. Am. Chem. Soc.*, 1971, **93**, 2534–2535.
17 A. C. Fahrenbach, J. C. Barnes, D. A. Lanfranchi, H. Li, A. Coskun, J. J. Gassensmith, Z. Liu, D. Benítez, A. Trabolsi, W. A. Goddard, M. Elhabiri and J. F. Stoddart, *J. Am. Chem. Soc.*, 2012, **134**, 3061–3072.
18 Y. Wang, J. Sun, Z. Liu, M. S. Nassar, Y. Y. Botros and J. F. Stoddart, *Chem. Sci.*, 2017, **8**, 2562–2568.
19 (*a*) A. F. Greene, M. K. Danielson, A. O. Delawder, K. P. Liles, X. Li, A. Natraj, A. Wellen and J. C. Barnes, *Chem. Mater.*, 2017, **29**, 9498–9508; (*b*) Z. Qian, X. Huang and Q. Wang, *Dyes Pigm.*, 2017, **145**, 365–370.
20 G. C. Granqvist, *Handbook of Inorganic Electrochromic Materials*, Elsevier, Amsterdam, 1995.
21 P. M. S. Monk, R. J. Mortimer and D. R. Rosseinsky, *Electrochromism and Electrochromic Devices*, Cambridge University Press, Cambridge, UK, 2007.
22 J. R. J. J. Platt, *J. Chem. Phys.*, 1961, **34**, 862–863.
23 J. W. Park, N. H. Choi and J. H. Kim, *J. Phys. Chem.*, 1996, **100**, 769–774.
24 P. A. Quintela and A. E. Kaifer, *Langmuir*, 1987, **3**, 769–773.
25 A. Trabolsi, N. Khashab, A. C. Fahrenbach, D. C. Friedman, M. T. Colvin, K. K. Cotí, D. Benítez, E. Tkatchouk, J. C. Olsen, M. E. Belowich, R. Carmielli, H. A. Khatib, W. A. Goddard III, M. R. Wasielewski and J. F. Stoddart, *Nat. Chem.*, 2010, **2**, 42–49.
26 H. J. Kim, W. S. Jeon, Y. H. Ko and K. Kim, *Proc. Natl. Acad. Sci. U. S. A.*, 2002, **99**, 5007–5011.
27 W. Ong, M. Gomez-Kaifer and A. E. Kaifer, *Org. Lett.*, 2002, **4**, 1791–1794.
28 W. S. Jeon, H. J. Kim, C. Lee and K. Kim, *Chem. Commun.*, 2002, 1828–1829.
29 J. W. Lee, S. Samal, N. Selvapalam, H. J. Kim and K. Kim, *Acc. Chem. Res.*, 2003, **36**, 621–630.
30 E. Pazos, P. Novo, C. Peinador, A. E. Kaifer and M. D. García, *Angew. Chem., Int. Ed.*, 2019, **58**, 403–416.
31 (*a*) K. Nchimi Nono, P. Dalvand, K. Wadhwa, S. Nuryyeva, S. Alneyadi, A. Fahrenbach, J. C. Olsen, Z. Asfari, C. Platas-Iglesias, M. Elhabiri and A. Trabolsi, *Chem.–Eur. J.*, 2014, **20**, 7334–7344; (*b*) K. Wadhwa, S. Nuryyeva, A. C. Fahrenbach, M. Elhabiri, C. Platas-Iglesias and A. Trabolsi, *J. Mater. Chem. C*, 2013, **1**, 2302–2307.
32 R. Kannappan, C. Bucher, E. Saint-Aman, J. C. Moutet, A. Milet, M. Oltean, E. Métay, S. Pellet-Rostaing, M. Lemaire and C. Chaix, *New J. Chem.*, 2010, **34**, 1373–1386.
33 W. Geuder, S. Huenig and A. Suchy, *Tetrahedron*, 1986, **42**, 1665–1667.
34 S. J. Atherton, K. Tsukahara and R. G. Wilkins, *J. Am. Chem. Soc.*, 1986, **108**, 3380–3385.
35 W. S. Abdul-Hassan, D. Roux, C. Bucher, S. Cobo, F. Molton, E. Saint-Aman and G. Royal, *Chem.–Eur. J.*, 2018, **24**, 12961–12969.
36 M. Berville, S. Choua, C. Gourlaouen, C. Boudon, L. Ruhlmann, C. Bailly, S. Cobo, E. Saint-Aman, J. A. Wytko and J. Weiss, *ChemPhysChem*, 2017, **18**, 796–803.
37 M. Berville, L. Karmazin, J. A. Wytko and J. Weiss, *Chem. Commun.*, 2015, **51**, 15772–15775.
38 A. Iordache, M. Retegan, F. Thomas, G. Royal, E. Saint-Aman and C. Bucher, *Chem.–Eur. J.*, 2012, **18**, 7648–7653.
39 S. Chowdhury, Y. Nassar, L. Guy, D. Frath, F. Chevallier, E. Dumont, A. P. Ramos, G. J. F. Demets and C. Bucher, *Electrochim. Acta*, 2019, **316**, 79–92.
40 A. Iordache, M. Oltean, A. Milet, F. Thomas, E. Saint-Aman and C. Bucher, *J. Am. Chem. Soc.*, 2012, **134**, 2653–2671.
41 M. Mohammad, *Electrochim. Acta*, 1988, **33**, 417–419.
42 T. G. Zhan, T. Y. Zhou, F. Lin, L. Zhang, C. Zhou, Q. Y. Qi, Z. T. Li and X. Zhao, *Org. Chem. Front.*, 2016, **3**, 1635–1645.
43 K. Madasamy and M. Kathiresan, *ChemistrySelect*, 2016, **1**, 354–359.
44 Y. Wang, M. Frasconi, W. G. Liu, Z. Liu, A. A. Sarjeant, M. S. Nassar, Y. Y. Botros, W. A. Goddard and J. F. Stoddart, *J. Am. Chem. Soc.*, 2015, **137**, 876–885.
45 J. Iehl, M. Frasconi, H. P. Jacquot de Rouville, N. Renaud, S. M. Dyar, N. L. Strutt, R. Carmieli, M. R. Wasielewski, M. A. Ratner, J. F. Nierengarten and J. F. Stoddart, *Chem. Sci.*, 2013, **4**, 1462–1469.
46 (*a*) A. Iordache, R. Kanappan, E. Métay, M. C. Duclos, S. Pellet-Rostaing, M. Lemaire, A. Milet, E. Saint-Aman and C. Bucher, *Org. Biomol. Chem.*, 2013, **11**, 4383–4389; (*b*) C. Kahlfuss, E. Métay, M. C. Duclos, M. Lemaire, M. Oltean, A. Milet, E. Saint-Aman and C. Bucher, *C. R. Chim.*, 2014, **17**, 505–511.
47 C. Kahlfuss, E. Metay, M. C. Duclos, M. Lemaire, A. Milet, E. Saint-Aman and C. Bucher, *Chem.–Eur. J.*, 2015, **21**, 2090–2106.
48 M. Elancheziyan, K. Theyagarajan, D. Saravanakumar, K. Thenmozhi and S. Senthilkumar, *Mater. Today Chem.*, 2020, **16**, 100274.
49 C. M. Ronconi, J. F. Stoddart, V. Balzani, M. Baroncini, P. Ceroni, C. Giansante and M. Venturi, *Chem.–Eur. J.*, 2008, **14**, 8365–8373.

© 2021 The Author(s). Published by the Royal Society of Chemistry

Open Access Article. Published on 02 September 2021. Downloaded on 4/18/2026 12:09:39 PM.
This article is licensed under a Creative Commons Attribution-NonCommercial 3.0 Unported Licence.

50 G. Das, T. Prakasam, S. Nuryyeva, D. S. Han, A. Abdel-Wahab, J. C. Olsen, K. Polychronopoulou, C. Platas-Iglesias, F. Ravaux, M. Jouiad and A. Trabolsi, *J. Mater. Chem. A*, 2016, **4**, 15361–15369.

51 M. Marchini, M. Baroncini, G. Bergamini, P. Ceroni, M. D'Angelantonio, P. Franchi, M. Lucarini, F. Negri, T. Szreder and M. Venturi, *Chem.–Eur. J.*, 2017, **23**, 6380–6390.

52 I. Thondorf, A. Shivanyuk and V. Bohmer, in *Calixarene, 2001*, ed. Z. Asfari, V. Bohmer, J. Harrowfield and J. Vicens, Kluwer Academic publisher, Dordrecht, 2001, vol. 2.

53 *Functional Synthetic Receptors*, ed. T. Schrader and A. D. Hamilton, Wiley-VCH, Weinheim, 2005.

54 K. Ariga and T. Kunitake *Supramolecular Chemistry-Fundamentals and Applications*, Springer, Berlin, 2005.

55 *Highlights in Bioorganic Chemistry: Methods and Applications*, ed. C. Schmuck and H. Wennemers, Wiley-VCH, Weinheim, 2004.

56 S. Kubik, C. Reyheller and S. Stuwe, *J. Inclusion Phenom. Macrocyclic Chem.*, 2005, **52**, 137–187.

57 H. C. Ko, S. A. Park, W. K. Paik and H. Lee, *Synth. Met.*, 2002, **132**, 15–20.

58 (*a*) S. Luan, Q. Ge, Y. Chen, M. Dai, J. Yang, K. Li, D. Liu and L. Zhao, *Bioorg. Med. Chem. Lett.*, 2017, **27**, 1943–1948; (*b*) W. Wang, C. Sheng, X. Che, H. Ji, Y. Cao, Z. Miao, J. Yao and W. Zhang, *Bioorg. Med. Chem. Lett.*, 2009, **19**, 5965–5969.

59 W.-W. Gu, W.-J. Chen and C.-G. Yan, *Supramol. Chem.*, 2015, **27**, 407–413.

60 R. Pomecko, PhD thesis University of Strasbourg, 2007.

61 Z. T. Li, G. Z. Ji, C. X. Zhao, S. D. Yuan, H. Ding, C. Huang, A. L. Du and M. Wei, *J. Org. Chem.*, 1999, **64**, 3572–3584.

62 Y. Zhao and D. G. Truhlar, *Theor. Chem. Acc.*, 2008, **120**, 215–241.

63 M. J. Frisch, G. W. Trucks, H. B. Schlegel, G. E. Scuseria, M. A. Robb, J. R. Cheeseman, G. Scalmani, V. Barone, G. A. Petersson, H. Nakatsuji, X. Li, M. Caricato, A. V. Marenich, J. Bloino, B. G. Janesko, R. Gomperts, B. Mennucci, H. P. Hratchian, J. V. Ortiz, A. F. Izmaylov, J. L. Sonnenberg, D. Williams-Young, F. Ding, F. Lipparini, F. Egidi, J. Goings, B. Peng, A. Petrone, T. Henderson, D. Ranasinghe, V. G. Zakrzewski, J. Gao, N. Rega, G. Zheng, W. Liang, M. Hada, M. Ehara, K. Toyota, R. Fukuda, J. Hasegawa, M. Ishida, T. Nakajima, Y. Honda, O. Kitao, H. Nakai, T. Vreven, K. Throssell, J. A. Montgomery Jr, J. E. Peralta, F. Ogliaro, M. J. Bearpark, J. J. Heyd, E. N. Brothers, K. N. Kudin, V. N. Staroverov, T. A. Keith, R. Kobayashi, J. Normand, K. Raghavachari, A. P. Rendell, J. C. Burant, S. S. Iyengar, J. Tomasi, M. Cossi, J. M. Millam, M. Klene, C. Adamo, R. Cammi, J. W. Ochterski, R. L. Martin, K. Morokuma, O. Farkas, J. B. Foresman, and D. J. Fox, *Gaussian 16, Revision B.01*, Gaussian, Inc., Wallingford CT, 2016.

64 (*a*) G. Scalmani and M. J. Frisch, *J. Chem. Phys.*, 2010, **132**, 114110; (*b*) J. Tomasi, B. Mennucci and R. Cammi, *Chem. Rev.*, 2005, **105**, 2999–3094.

65 A. S. Jalilov, S. Patwardhan, A. Singh, T. Simeon, A. A. Sarjeant, G. C. Schatz and F. D. Lewis, *J. Phys. Chem. B*, 2014, **118**, 125–133.

66 A. Alberti, in *Organic Photochromic and Thermochromic Compounds*, ed. J. C. Crano and R. J. Guglielmetti, Kluwer Academic publisher, 2002, 4, pp. 211–240.

67 W. L. Mock and N.-Y. Shih, *J. Org. Chem.*, 1986, **51**, 4440–4446.

68 B. Perlmutter-Hayman, *Acc. Chem. Res.*, 1986, **19**, 90–96.

69 C. Lee, M. S. Moon and J. W. Park, *J. Electroanal. Chem.*, 1996, **407**, 161–167.

70 J. F. Stargardt and F. M. Hawkridge, *Anal. Chim. Acta*, 1983, **146**, 1–8.

71 P. M. S. Monk, N. M. Hodgkinson and S. A. Ramzan, *Dyes Pigm.*, 1999, **43**, 207–217.

© 2021 The Author(s). Published by the Royal Society of Chemistry